(18) D. R. Lide, D. E. Mann, and R. M. Fristrom, *J. Chem. Phys.*, **26**, 736 (1957).
(19) S. Rothenberg and H. F. Schaefer, *J. Chem. Phys.*, **53**, 3014 (1970).
(20) L. S. Cederbaum, W. Domcke, W. von Niessen, and W. P. Kraemer, *Mol. Phys.*, **34**, 381 (1977).
(21) D. W. Turner, C. Baker, A. D. Baker, and C. R. Brundle, "Molecular Photoelectron Spectroscopy", Wiley-Interscience, London, 1970.
(22) The Xα SW calculations are, however, much less demanding on computer time. The full Xα SW calculation (in double precision) for SO_2, including the initial energy level determination, required 130 s on an IBM 370/168 computer. The near-Hartree–Fock calculations required about 7 h on a Univac 1108, a machine that is about 7 times slower. For SO_2, the Xα SW calculations are made in about one-thirtieth of the equivalent time required for the near-Hartree–Fock calculations, but for larger molecules the absolute savings in computation times are much greater with the Xα SW method.
(23) I. H. Hillier and V. R. Saunders, *Trans. Faraday Soc.*, **66**, 1544 (1970).
(24) The Mulliken charge distributions for the various restricted-basis-set calculations for SO_2 vary widely. This reflects both the real differences in the calculations and also the arbitrary aspects of the population analyses. From ref 19 and 23 representative atomic charges on S are +0.82 minimal s,p basis, +0.14 minimal s,p,d basis, +1.35 extended s,p basis, and +1.13 extended s,p,d basis. The calculated dipole moments according to these calculations are 1.24, 0.81, 2.83, and 2.28 D, respectively, and these values are to be compared with the experimental value of 1.63 D.
(25) D. R. Lide, D. E. Mann, and J. J. Comeford, *Spectrochim. Acta*, **21**, 497 (1965).
(26) M. W. Dougill, *J. Chem. Soc.*, 3211 (1963).

Contribution from the Chemistry Department, University of Texas, Austin, Texas 78712

Instabilities in the Elpasoite Structure: Structural-Phase Transformations and the Temperature-Dependent Raman Spectra of $Cs_2LiCo(CN)_6$ and $Cs_2LiIr(CN)_6$

B. I. SWANSON* and B. C. LUCAS

Received March 1, 1978

The structural-phase transformations in $Cs_2LiCo(CN)_6$ and $Cs_2LiIr(CN)_6$ have been probed using Raman scattering and optical microscopy. The goal of the present work has been to describe the structural distortions in terms of the allowed modes of vibration in the high-temperature cubic phase. The Ir^{3+} salt undergoes two phase transformations (T_c^1 = 418 K, T_c^2 = 335 K) while the Co^{3+} salt is observed optically to have one phase change (T_c^1 = 183 K). The 418 K phase change in the Ir^{3+} salt is first order involving rotation of the $Ir(CN)_6^{3-}$ octahedra. The 335 K transition is second order with the structural distortion proceeding along a soft Cs^+ translational mode. The phase transformation in $Cs_2LiCo(CN)_6$ involves a simultaneous distortion along the same two phonons. The structural instabilities for these two salts are the same as those observed earlier for other $R_2MM'L_6$ salts indicating that materials with the elpasoite structure may share a common lattice instability. The transition temperatures for $Cs_2LiM(CN)_6$ (M = $Cr^{3+} \rightarrow Co^{3+}$) salts correlate with the size of the Cs^+ site, as is consistent with the earlier suggestion that the driving force for the instabilities in these materials results from Cs^+ atoms occupying too large a site in the cubic lattice. As the Cs^+ site size decreases, the high-temperature cubic cell is stabilized thereby lowering the critical temperatures for the phase transformations. The correlation of Cs^+ site size and the critical temperature is not maintained in comparison of the Cr^{3+} and Ir^{3+} salts. The unusual behavior of the Ir^{3+} material has been attributed to a cooperative interaction of the external phonon instabilities with the internal forces of the $Ir(CN)_6^{3-}$ complex ion.

Displacive-phase transformations in crystalline solids have gained prominence in recent years, largely as a result of the compelling simplicity of the dynamics of second-order transitions.[1-3] The structural distortion accompanying a second-order displacive-phase change, the parallel to a reaction path for a chemical transformation, proceeds along one phonon direction in the vicinity of the critical temperature.[1,2] Furthermore, the structural distortion is continuous with temperature, thereby allowing the "reaction path" to be followed experimentally. The dynamics of chemical transformations, in addition to being considerably more complex, cannot be directly probed by experiment.

While there have been numerous studies of the dynamics of structural-phase changes in simple systems, such as the perovskites,[3,4] less is known of the lattice instabilities in more complex materials. We have been interested in salts containing octahedrally coordinated ML_6^{n-} complex ions, where the nature of the complex ion may influence the lattice instability.[5-8] Our principal goal in these studies has been to describe the dynamics of the structural change in terms of the allowed crystalline modes of vibration. Several temperature-dependent NQR studies of R_2MX_6 salts possessing the antifluorite structure (K_2PtCl_6,[9] K_2PdCl_6,[9] K_2IrCl_6,[9] K_2ReCl_6,[10-14] $(NH_4)_2PtBr_6$,[15] K_2PtBr_6,[17] K_2OsCl_6,[17] and K_2SnCl_6[18,19]) have been reported. These materials are observed to undergo multiple phase changes as temperature is lowered, and the NQR studies clearly indicate that the first transition in each involves rotation of the MX_6^{2-} octahedra. The lower temperature transformations are not well understood. However, we recently reported the temperature-dependent Raman scattering for K_2SnBr_6 in which a soft translational mode was implicated in the second phase change at 368 ± 5 K.[8] The first phase change in K_2SnBr_6 (T_c^1 = 399 K) involves rotation of the $SnBr_6^{2-}$ octahedra, as is consistent with the NQR studies of other antifluorite materials.[9-19]

The high-temperature phase of the antifluorite salts (cubic, *Fm3m*) is closely related to the elpasoite structure ($R_2MM'L_6$) adopted by many octahedrally coordinated trivalent metals. The antifluorite and elpasoite structures are identical except for the addition of the univalent M^+ cation in the 4b octahedral hole in the *Fm3m* cell of the latter. Salts with the elpasoite structure have been probed extensively in the past decade by workers interested in the structure and spectroscopy of ML_6^{3-} complex ions. The advantage of the $R_2MM'L_6$ salts in such studies is that the ML_6^{3-} ion occupies a site with O_h symmetry. Salts with three common cations, $M_3M'L_6$, generally have much lower symmetry. However, while high symmetry has made $R_2MM'L_6$ salts the preferred materials for studies of complexes of trivalent metals, few workers have worried about structural-phase transformations which may occur for elpasoites at reduced temperatures, despite the fact that many spectroscopic studies are carried out at low temperatures.

0020-1669/78/1317-2717$01.00/0

Table I

elpasoite salt	lattice parameters (cubic phase)	Cs–N interatomic dist, Å	Cs–C interatomic dist, Å	T_c^1, K	T_c^2, K	Cs^+ amplitude of vib, Å
$Cs_2LiIr(CN)_6$	$a = 10.720$ (3) Å	3.817 (1)	3.850 (1)	418	335	0.287 (1)
$Cs_2LiCr(CN)_6$	$a = 10.780$ (2) Å	3.842 (1)	3.866 (1)	348	310	0.263 (1)
$Cs_2LiMn(CN)_6$	$a = 10.667$ (3) Å	3.798 (1)	3.834 (1)	273 (±10)[a]		0.232 (2)
$Cs_2LiFe(CN)_6$	$a = 10.571$ (2) Å	3.762 (1)	3.805 (1)	221	170	0.216 (1)
$Cs_2LiCo(CN)_6$	$a = 10.495$ (1) Å	3.733 (1)	3.783 (1)	183[b]	168[b]	0.205 (1)

[a] Only one phase change discernible optically. [b] The 183 K transition was observed optically while the soft mode ($\tilde{\nu}^2$ vs. T (K)) extrapolation resulted in a critical temperature of 168 K.

While there have been relatively few studies of lattice instabilities in elpasoite materials, the phase transformations exhibited by $Cs_2LiCr(CN)_6$ have been well characterized.[5] The chromicyanide material undergoes two phase transformations above room temperature. The first of these (T_c^1 = 348 K, $Fm3m \rightarrow P4/mnc$) involves an antiferrodisplacive rotation of the $Cr(CN)_6^{3-}$ octahedra about the c axis of the cubic cell. Essentially, the structural change involves a distortion along the A_{2g} component of the $Cr(CN)_6^{3-}$ rotary mode at the Brillouin zone boundary (X point). The second phase change at 310 K results from a soft Cs^+ translational mode condensing out at the X point relative to the cubic cell.

There are clear indications that the instabilities exhibited by $Cs_2LiCr(CN)_6$ may be general for the large class of materials possessing the elpasoite structure. Raman studies show that similar phase transformations occur for $Cs_2MFe(CN)_6$ (M = Mg^{2+}, Ca^{2+}, Sr^{2+}, and Ba^{2+}),[7] $Cs_2MFe(CN)_6$ (M = Li^+, Na^+, and K^+),[6,20] and $Cs_2NaLnCl_6$ (Ln = lanthanide).[21] Furthermore, there is evidence that the critical temperatures of the phase transformations are directly related to the size of the Cs^+ ion site in the $Fm3m$ cell.[7] Indeed, the instabilities in these materials appear to result from the Cs^+ ion occupying a site which is too large.[5] A correlation between the relative ion/site size and critical temperatures have also been noted for the cell doubling transition in the cubic perovskites.[22]

The utility of knowing more about structural instabilities in elpasoites is clear; a priori knowledge of which cations and which temperatures are required to ensure that the ML_6^{3-} ion is in an octahedral site would be extremely useful. The present study of the phase transformations in $Cs_2LiCo(CN)_6$ and $Cs_2LiIr(CN)_6$ was initiated to further probe the generalities underlying the structural instabilities in elpasoites. Correlations with $Cs_2LiCr(CN)_6$ are of interest here since the Cs^+ site size is observed to decrease in proceeding along the series $Cr^{3+} \rightarrow Ir^{3+} \rightarrow Co^{3+}$.[23]

Experimental Section

The dicesium lithium salts $Cs_2LiCo(CN)_6$ and $Cs_2LiIr(CN)_6$ were prepared by combining stoichiometric molar ratios of $Cs_3M(CN)_6$ and $Li_3M(CN)_6$, M = Co^{3+}, Ir^{3+}. The tricesium and trilithium salts were initially prepared from the tripotassium salts by ion exchange using hydrogen form resin with ^1H replaced by Li or Cs (Bio-Rad, AG 50W-X16).[23] The potassium salt of Ir^{3+} was obtained from Alfa and the Co^{3+} salt prepared using the usual literature preparation.[24] Single crystals of the Co^{3+} and Ir^{3+} salts were obtained by slow evaporation of aqueous solutions as well as slow diffusion of ethanol into aqueous solutions of the salts.

Raman data from 20 to 298 K were obtained using a Cary 82 spectrometer and the red and yellow lines (6471 and 5682 Å) of a Spectra Physics 164 Kr^+ ion laser. Crystals were coupled with Crycon grease to a copper cold finger of an Air Products Displex closed-cycle He cryostat. The temperature was monitored using a constantan thermocouple attached to the copper plate. High-temperature Raman data (300 → 470 K) were obtained using a crystal mounted on a glass fiber. The temperature of the crystal was controlled using a dry N_2 gas stream. Raman scans were obtained with the incident radiation oriented along the (001) and (101) crystallographic directions. Scans obtained using these two orientations were essentially the same, except for slight variations on the relative intensities. The figures presented here were taken from the (100) orientation scans. Visual alignment was sufficient since the crystals exhibit regular cubic morphologies. The crystals used in the Raman experiments ranged from 1.25 to 0.4 mm on edge.

Optical microscopic observations were made using two apparatus. The high-temperature observations ($T > 300$ K) were made using a Zeiss polarizing microscope and a Mettler FP-3 thermal stage for temperature control. Observations below room temperature were performed using a Nikon SBR-KT polarizing microscope with the crystal temperature controlled by a cold N_2 gas stream. The crystals were mounted on glass fibers with silicone adhesive for the low-temperature studies. Experiments were also performed with the crystals placed in a small glass container so as to obviate strain effects in the transition temperature. The critical temperatures were the same for both experiments. The low-temperature devices for the Raman and optical microscopic experiments were calibrated using crystalline samples with known phase changes.

Results

Optical microscopy provides one means of establishing the critical temperatures for the phase transformations in the $Cs_2LiM(CN)_6$ salts. The first phase change in the $Cs_2LiCr(CN)_6$ salt (cubic → tetragonal) is characterized by a sharp isotropic–nonisotropic change in the transmission of polarized light.[5] The second-order phase change, while more subtle, was also easily detected. In a similar manner, two structural changes are clearly discernible for the Ir^{3+} salt. The sharpness of the optical change in $Cs_2LiIr(CN)_6$ at 418 K is suggestive of a first-order phase change. The Mn^{3+} and Co^{3+} salts when viewed optically as a function of temperature exhibit only one distinguishable phase change. In the Co^{3+} salt the phase transformation is characterized by a distinct optical change in the crystal at approximately 183 K. While no other phase change could be detected for $Cs_2LiCo(CN)_6$ optically (to ca. 120°K) the critical temperature obtained from the temperature dependence of the soft mode (below) is 15 K lower than that observed optically, suggesting the presence of a second phase change slightly below 183 K. The Mn^{3+} salt exhibits a more subtle optical change at 273 ± 10 K. The critical temperatures of the $Cs_2LiM(CN)_6$ compounds are given in Table I.

The vibrational selection rules for the $Fm3m$ phase of the $Cs_2LiM(CN)_6$ materials have been given elsewhere.[25] In addition to the six $M(CN)_6^{3-}$ internal modes expected in the Raman spectra (2 A_{1g}, 2 E_g, and 2 F_{2g}) there is one Raman-active translational mode (F_{2g}, Cs^+ ion). The rotary mode is inactive in the cubic phase.

It is also pertinent to review the selection rules for the two low-temperature phases of the $Cs_2LiCr(CN)_6$ salt. The $M(CN)_6^{3-}$ and Li^+ ions occupy sites with inversion symmetry in both $P4/mnc$ and $P2_1/n$. Thus, internal modes which are symmetric to inversion in $Fm3m$ will remain so in the lower temperature phases. Essentially, infrared-active modes in $Fm3m$ (excepting the F_{1u} Cs^+ translation) will not be Raman active in either low-temperature phase. Furthermore, translational modes which are Raman active in $Fm3m$, $P4/mnc$, or $P2_1/n$ must involve Cs^+ motion exclusively, since translation of either $M(CN)_6^{3-}$ or Li^+ ions will destroy the inversion symmetry. It is also important to note that the F_{1u}

Table II. Vibrational Selection Rules for $Cs_2LiM(CN)_6$ in $P4/mnc$ and $P2_1/n$

$M(CN)_6^{3-}$ Modes

$P2_1/n$ space group			$P4/mnc$ space group	
factor group sym C_{2h}	site sym C_i	free ion sym O_h	site sym C_{4h}	factor group sym D_{4h}
$A_g + B_g$	A_g	A_{1g}	A_g	$A_{1g} + A_{2g}$
$2A_g + 2B_g$	$2A_g$	E_g	A_g	$A_{1g} + A_{2g}$
			B_g	$B_{1g} + B_{2g}$
$3A_g + 3B_g$	$3A_g$	F_{1g}	A_{1g}	$A_{1g} + A_{2g}$
			E_g	$2E_g$
$3A_u + 3B_u$	$3A_u$	F_{1u}	A_u	$A_{1u} + A_{2u}$
			E_u	$2E_u$
$3A_g + 3B_g$	$3A_g$	F_{2g}	B_g	$B_{1g} + B_{2g}$
			E_g	$2E_g$
$3A_u + 3B_u$	$3A_g$	F_{2u}	B_u	$B_{1u} + B_{2u}$
			E_u	$2E_u$

External Modes

$P2_1/n$ space group		$P4/mnc$ space group	
translatory	rotary	translatory	rotary
$3A_g$ (Cs^+)	$3A_g$	A_{2g} (Cs^+)	A_{1g}
$3B_g$ (Cs^+)	$3B_g$	B_{1g} (Cs^+)	A_{2g}
$8A_u$ (Cs^+, Li^+, M)		$2E_g$ (Cs^+)	$2E_g$
$7B_u$ (Cs^+, Li^+, M)		$2A_{1u}$ (M, Li^+)	
		$2A_{2u}$ (M, Li^+, Cs^+)	
		B_{1u} (Cs^+)	
		$5E_u$ (M, Li^+, Cs^+)	

Table III. Observed Raman Modes (cm^{-1}) for $Cs_2LiCo(CN)_6$ and $Cs_2LiIr(CN)_6$ at various temperatures

sym and approx descripts		$Cs_2LiCo(CN)_6$		$Cs_2LiIr(CN)_6$		
$Fm3m$	$P4/mnc$	20 K	298 K	22 K	147 K	298 K
$\nu_1(A_{1g}$, CN str)		2166.8	2161.1	2183.7	2181.1	2180.0
$\nu_2(A_{1g}$, MC str)		433.3	420.1	461.2	460	458
$\nu_3(E_g$, CN str)		2155.1	2150.8	2161.0	2157.8	2157.7
				2157.8		
$\nu_4(E_g$, MC str)		421.1	418.1	461.2	460	458
$\nu_{10}(F_{2g}$, MCN)		486.7	484.6	483.7	484	483
$\nu_{11}(F_{2g}$, CMC)		194	189.9	189.3	183.5	181
				183.5	171.1	
				177.5		
		114.4		121.9	116.3	101.5
$\nu_{14}(F_{1g}$, rot)	E_g	103.7		105.7	102.4	
	A_{1g}	65.0				
$\nu_{16}(F_{1u}$, Cs^+)	A_{2g}			53.4		
$\nu_{17}(F_{2g}$, Cs^+)	E_g	46.3	40.5	49.7		
		44.4		47.7	45.5	42.5
$\nu_7(F_{2g}$, Cs^+) soft mode	B_{1g}	34.6		41.5	36.6	30.7
(ν_{16}, Cs^+)	E_g	28.3		30.9	25.5	

symmetry Cs^+ translational mode in $Fm3m$ will become Raman active in the two low-temperature phases since the primitive cell is doubled and since the Cs^+ is not on an inversion center in $Fm3m$. The rotary modes will become active in both low-temperature phases. The low-energy ($\bar{\nu} < 150$ cm^{-1}) Raman selection rules in the two low-temperature phases are, therefore, reasonably simple; 6 rotary ($3A_g + 3B_g$) and 6 Cs^+ translational modes ($3A_g + 3B_g$) are expected in $P2_1/n$ while 3 rotary ($A_{1g} + 2E_g$) and 3 translational modes ($B_{1g} + 2E_g$) are expected in $P4/mnc$. The selection rules are presented in Table II.

The simplicity of the low-energy Raman spectrum in the cubic phase, where $\nu_{17}(Cs^+, F_{2g}) \approx 40$ cm^{-1} and ν_{11}(C–M–C, δF_{2g}) ≈ 180 cm^{-1}, is lost in going to low temperatures. The region below 200 cm^{-1} is depicted as a function of temperature for the Ir^{3+} material in Figure 1. A new peak appears on the low-energy side of ν_{17} immediately below the first critical

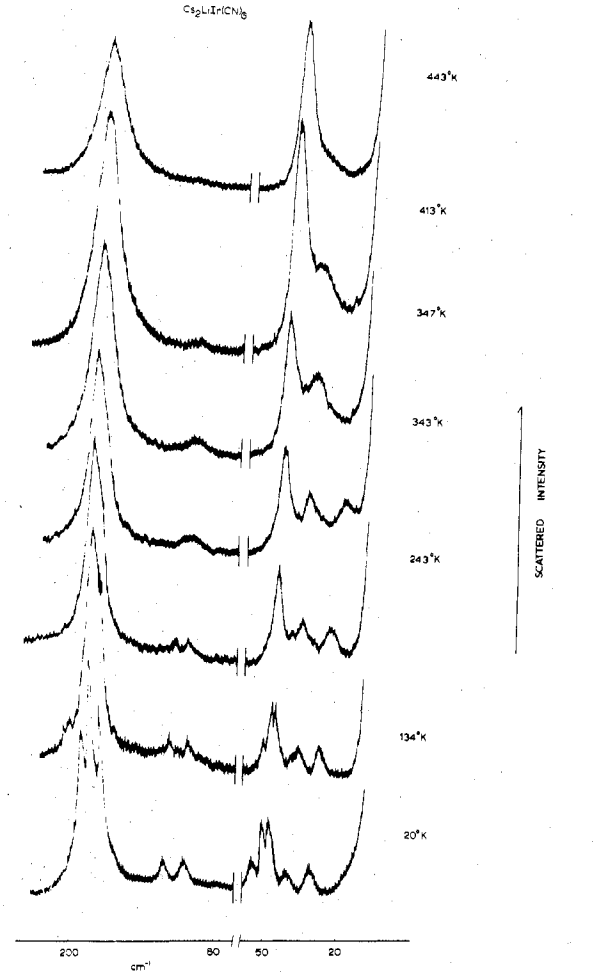

Figure 1. Temperature-dependent Raman scattering below 200 cm^{-1} for $Cs_2LiIr(CN)_6$.

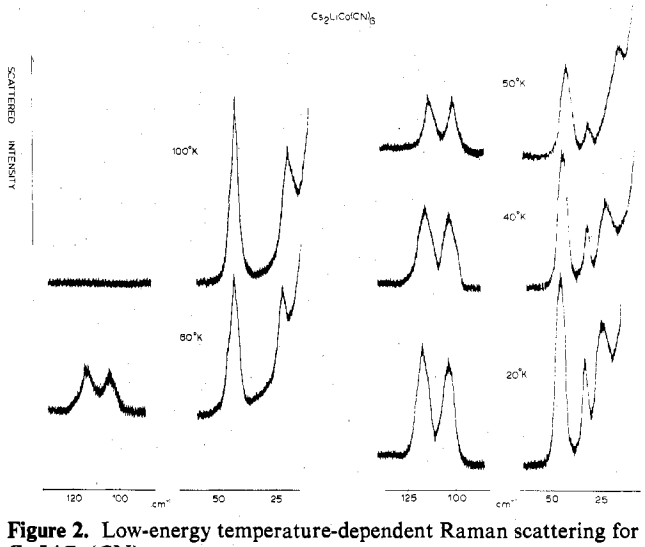

Figure 2. Low-energy temperature-dependent Raman scattering for $Cs_2LiCo(CN)_6$.

temperature of the salt. Upon further cooling (well below T_c^2 for the Ir^{3+} material) a new feature emerges from the exciting line hardening to 31 cm^{-1} at 20 K. The same trend is observed for the Co^{3+} salt with the last feature (soft mode) hardening to 28.4 cm^{-1} (Figure 2). At extremely low temperatures the Ir^{3+} spectra show ν_{17} to split into two components and a new band to emerge at approximately 53 cm^{-1}.

In addition to the bands below 60 cm^{-1}, new peaks are observed around 110 cm^{-1} immediately below T_c^1 for both

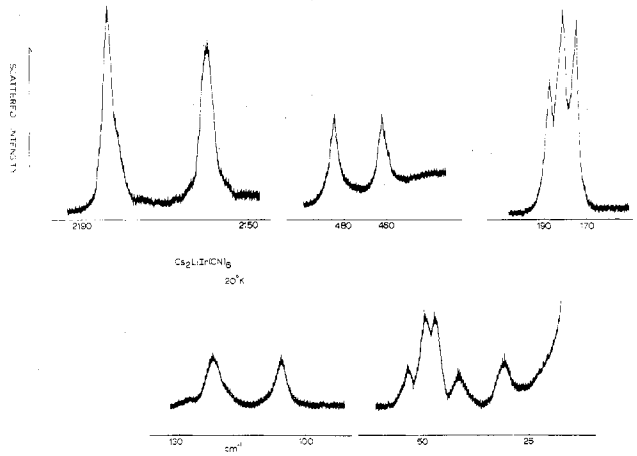

Figure 3. Raman scattering for $Cs_2LiIr(CN)_6$ at 20 K.

salts. The broad weak feature first observed upon entering phase II splits into two bands at low temperature. Both features appear to increase in frequency as temperature is lowered; the temperature dependence of these features in the Ir^{3+} material is shown in Figure 1.

The regions above 150 cm^{-1}, where the $M(CN)_6^{3-}$ internal modes are expected, also exhibit temperature dependence. The C–Ir–C deformation at ca. 180 cm^{-1} splits into three well-resolved bands at low temperature (Figures 3 and 4). Similarly, the doubly degenerate C–N stretch, ν_3 (E_g, C–N), splits into two bands. The chromium salt exhibits similar splittings at low temperature. The degenerate modes of the Co^{3+} salt do not show such extensive splitting, although ν_{11} does become asymmetric at low temperature. It should be noted that the critical temperature for the Co^{3+} salts is much lower than those of the Ir^{3+} or Cr^{3+} salts.

The observed Raman spectra of the Cr^{3+} and Ir^{3+} salts indicate that the assignments proposed earlier for ν_2 (A_{1g}, MC stretch) and ν_{10} (F_{2g}, MCN δ)[25] may be reversed for the Ir^{3+} salt. All of the stretching modes in $Cs_2LiCr(CN)_6$ are observed to shift to slightly higher frequencies as temperature is reduced. The frequencies of the C–N stretching modes in the Ir^{3+} salt are also observed to increase upon cooling. However, the 483-cm^{-1} feature originally assigned to M–C stretch does not shift appreciably upon cooling, while the 458-cm^{-1} band does. Thus, we prefer to assign the 483-cm^{-1} feature to ν_{10} and the 460-cm^{-1} band to ν_2. The observed band shapes (Figures 3 and 4) are also consistent with this assignment since the M–C stretching modes are generally sharp, while the MCN deformations are often broad at room temperature. The temperature-dependent spectra for $Cs_2LiIr(CN)_6$ show no evidence for the E_g symmetry M–C stretch (ν_4) in the 400–500-cm^{-1} region. It is possible that this mode is underneath the more intense ν_1 or is simply too weak to be observed. The alternative assignment of the 480-cm^{-1} feature as ν_4 is unreasonable since the E_g symmetry M–C stretch in hexacyanides has always been observed to have lower frequency than the symmetric M–C stretch, ν_2.

Assignment of the Low-Energy Modes

The temperature dependence of the Raman scattering for the Co^{3+} and Ir^{3+} salts is essentially the same as that observed earlier for the Cr^{3+} material.[5] Thus, the assignments for the cobalt and iridium salts will be based on the known phase II and phase III space groups of $Cs_2LiCr(CN)_6$. Throughout this discussion, the symmetry notation for the phase II $P4/mnc$ cell will be used.

The features which appear around 110 cm^{-1} in phase II, eventually splitting into two well-resolved peaks at low temperatures, must be attributed to $M(CN)_6^{3-}$ rotary modes. The only other Raman-active phonons in the low-energy

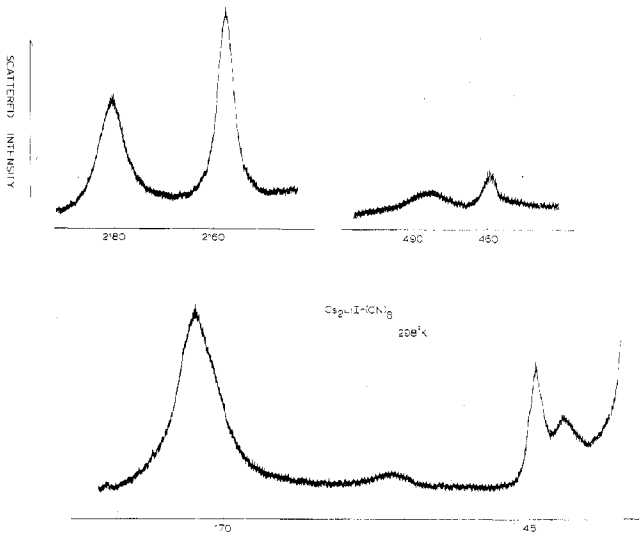

Figure 4. Raman scattering for $Cs_2LiIr(CN)_6$ at 298 K.

region, Cs^+ ion translations, are expected below 60 cm^{-1}. Furthermore, in a recent normal-mode analysis of $Cs_2LiCo(CN)_6$, where interionic potentials were included in the analysis, the $Co(CN)_6^{3-}$ rotary mode was predicted to be around 100 cm^{-1}.[26] We attribute both bands above 100 cm^{-1} to the two E_g components of the rotary mode. A third weak band observed at ca. 85 cm^{-1} (20 K) for the Cr^{3+} salt was also attributed to $Cr(CN)_6^{3-}$ rotation. This band was not observed in the Ir^{3+} salt but was seen in the Co^{3+} salt as a very weak band at 65 cm^{-1}. We attribute the 85-cm^{-1} and 65-cm^{-1} bands in $Cs_2LiCr(CN)_6$ and $Cs_2LiCo(CN)_6$, respectively, to the A_{1g} component of the $M(CN)_6^{3-}$ rotations. This latter mode, which represents antiferrodisplacive rotation about the cubic C axis, is expected to exhibit softening as T_c^1 is approached from below, since the mode defines the first phase change. Indeed, consideration of the positioning of the Cr^{3+} and Co^{3+} rotary modes at 85 and 65 cm^{-1}, respectively, supports this expectation. Noting the first-order transition temperature for the Co^{3+} and Cr^{3+} salts (183, 348 K), one observes the Co^{3+} salt at 20 K to be closer to its transition temperature, T_c^1, than the Cr^{3+} salt at 20 K is to its T_c^1. Thus, the Co^{3+} rotary mode (65 cm^{-1}) is expected to be and clearly is lower in frequency than the Cr^{3+} rotary mode (85 cm^{-1}) indicating a general softening of the mode as T_c^1 is approached.

The band which appears on the low-frequency side of ν_{17} was previously attributed to the A_{2g} component of the F_{1u} symmetry Cs^+ translation, ν_{16}.[5] In the present study this feature was detected for Ir^{3+} immediately upon entering phase II. Inasmuch as the A_{2g} component of ν_{16} is inactive in $P4/mnc$ (Table II) we prefer to assign this band to the B_{1g} component of ν_{17} (F_{2g}, Cs^+). We attribute the weak feature which appears to grow in at ca. 53 cm^{-1} (Figure 2) to the A_{2g} component of ν_{16}. This latter assignment seems reasonable since the A_{2g} component of ν_{16} will only become active in the phase III $P2_1/n$ cell. It should be noted that in the cubic phase ν_{16} is observed in the infrared spectra of the $Cs_2LiM(CN)_6$ salts around 50 cm^{-1}.[25]

The most intense feature in the region below 60 cm^{-1} is the F_{2g} symmetry Cs^+ translation. This band hardens as temperature is lowered eventually splitting into two well-resolved components (Figure 5). We attribute this band to the E_g component of ν_{17}. The remaining, and most important, band observed in these salts is the soft mode. By analogy with the Cr^{3+} salt we attribute the soft mode to the E_g component of ν_{16}. While the soft mode observed in the Cr^{3+} spectra split at extremely low temperatures (as is consistent with lifting the degeneracy in going to the $P2_1/n$ cell), no such splittings were

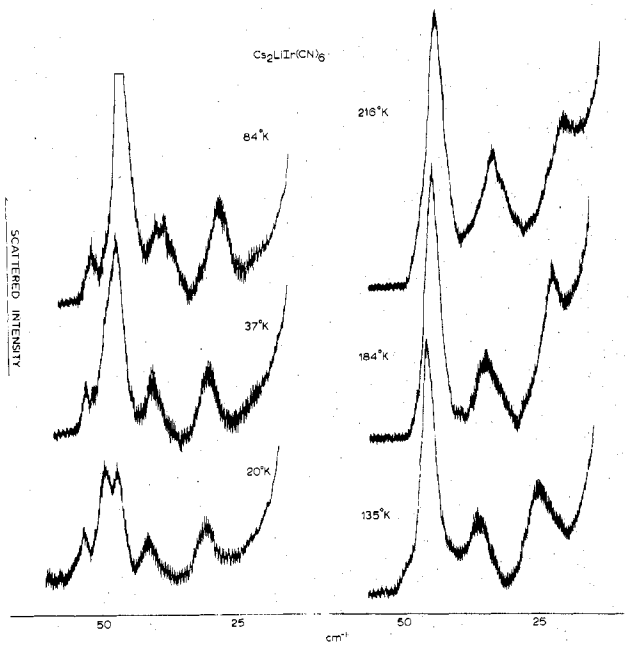

Figure 5. Temperature-dependent Raman scattering of $Cs_2LiIr(CN)_6$ in the low-energy (60 cm^{-1}) region.

observed for the Co^{3+} and Ir^{3+} salts.

With the above assignments, all six of the expected Cs^+ translations in $P2_1/n$ are observed. However, only three of the six expected rotary modes have been observed (only two for Ir^{3+}). The splitting pattern of the F_{1g} rotary mode is similar to that of the triply degenerate $M(CN)_6^{3-}$ internal modes. For example, while six components (3 A_g + 3 B_g) are expected for the F_{2g} symmetry C–M–C deformation at ca. 180 cm^{-1}, only three are observed at low temperatures. It is stressed that of the six Cs^+ translations observed at low temperatures, three result from ν_{17} (F_{2g}, Cs^+) while the other three eminate from ν_{16} (F_{1u}, Cs^+).

The low-frequency modes of the Co^{3+} salt exhibit unusual intensity changes in the temperature range $120 > T > 50$ K (Figure 2). The B_{1g} component of ν_{17} disappears in this temperature range while the soft mode gains considerable intensity. When crystals are cooled below 50 K the B_{1g} ν_{17} mode reappears and the intensity of the soft mode decreases. These changes are reversible with temperature. In addition, polarization of scattered radiation is scrambled in this temperature range. For example, the relative intensities of $z(xx)y$ and $z(xz)y$ scans of the C–N stretches change markedly upon cooling below 120 K. The origin of these unusual changes is not clear; although, it is possible that there is an additional phase change (involving, perhaps, orientational disorder) for the cobalt salt at low temperatures.

Discussion

Temperature-dependent Raman spectra as well as optical microscopic studies of the $Cs_2LiCo(CN)_6$ and $Cs_2LiIr(CN)_6$ clearly indicate the presence of phase transitions in these crystals. High-temperature Raman spectra ($T > 418$ K) for the Ir^{3+} show the modes expected for an $Fm3m$ lattice. As temperature is lowered new bands appear and several of the features which were present in the high-temperature spectra split, as is consistent with a change in symmetry as caused by the phase transitions. At room temperature $Cs_2LiIr(CN)_6$ has already undergone two phase transitions ($T_c^1 = 418$ K, $T_c^2 = 335$ K) and exhibits significant deviation from cubic selection rules. (See Table II and Figure 1.) Surprisingly, the room-temperature X-ray diffraction pattern for the Ir^{3+} salt is consistent with an $Fm3m$ cell. There are two possible sources for the erroneous data obtained from the X-ray

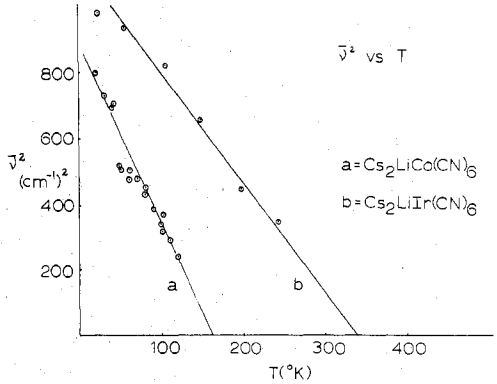

Figure 6. $\bar{\nu}^2$ vs. temperature for $Cs_2LiIr(CN)_6$ and $Cs_2LiCo(CN)_6$.

diffraction pattern. First, while two phase changes have definitely occurred before room temperature, the new reflections may be too weak to be observed in the presence of the strong scattering from the heavy Ir^{3+} atom. However, it should be noted that non-$Fm3m$ reflections were easily observed in the Cr^{3+} salt despite the fact that the critical temperatures were much closer to 300 K. A second possibility is that the long range order in the Ir^{3+} salt has been destroyed in going through the two phase changes. Any reflections may then be too diffuse to be observed. This example of the inability of X-ray diffraction to correctly predict structural changes should emphasize the extreme importance of employing varied techniques in studying structural instabilities. Raman spectroscopy is an especially powerful tool in this case since lack of long range order does not obscure such subtle distortions.

The similarity of the temperature dependent Raman scattering for the Cr^{3+}, Co^{3+}, and Ir^{3+} salts shows that the structural instabilities for all three materials are essentially the same. Raman spectroscopy is especially useful in clarifying the second-order phase changes in these materials. All three materials exhibit a strongly temperature-dependent Raman mode which merges with the exciting line as temperature is raised. A detailed plot of the region below 50 cm^{-1} is depicted in Figure 5. A plot of the square of the frequency of this mode as a function of temperature (Figure 6) shows the typical soft mode behavior expected for a second-order phase change. Extrapolation of $[\bar{\nu}(cm^{-1})]^2$ to zero phonon frequency provides an estimate of the critical temperature of the second-order phase change. The critical temperature obtained in this manner for the Ir^{3+} salt corresponds exactly with that obtained for the second phase change via optical microscopy (Figure 6, Table I). For the cobalt salt the critical temperature obtained from the soft mode frequency data (ca. 168 K) is slightly lower than the critical temperature observed optically for the first phase change ($T_c^1 = 183$ K). We conclude that structural changes corresponding to the first and second phase transformations in $Cs_2LiCr(CN)_6$ occur at essentially the same temperature in the cobalt salt.

The assignment of the soft mode is crucial to a proper description of the dynamics of a second-order phase change. Fortunately, the soft mode assignment in the $Cs_2LiM(CN)_6$ salts is unambiguous (Results section). The low frequency of the soft mode in these materials eliminates the $M(CN)_6^{3-}$ internal and rotary modes from consideration leaving only translational lattice modes. If one assumes that the lower temperature phase space groups for the Co^{3+} and Ir^{3+} salts are the same as those observed for $Cs_2LiCr(CN)_6$, the possibilities are further reduced to Cs^+ ion translations. From the splitting patterns and temperature dependence of the modes below 60 cm^{-1} it is clear that the soft mode involves an antiferrodisplacive translation of the Cs^+ ions along the (110) direction of the cubic cell. Essentially, all of the Cs^+ atoms

at $z = {}^1/_4$ translate along $(x + y)$ while those at $z = {}^3/_4$ translate along $(-x - y)$. A distortion along this phonon direction results in a doubling of the cubic cell, since the Cs^+ atoms at $z = {}^1/_4$ and $z = {}^3/_4$ are no longer symmetry equivalent.

Information concerning the first phase change in the Ir^{3+} salt is not definitive. However, the similarity of the Raman spectra and optical properties of the Ir^{3+} and Cr^{3+} salts indicates that the structural distortions are the same for both materials. In particular, rotary modes are observed above 100 cm^{-1} immediately upon cooling below T_c^1. Thus, we conclude that the first phase change in $Cs_2LiIr(CN)_6$ is first order involving rotation of the $Ir(CN)_6^{3-}$ moiety about the cubic c axis. Again, the structural change is most likely antiferrodisplacive, with the $Ir(CN)_6^{3-}$ octahedra at $z = 0$ and $z = {}^1/_2$ rotating in opposite directions. The Raman data obtained for the cobalt salt indicate a similar rotary instability. The only difference between these two salts is that distortions along both the rotary and Cs^+ translational modes occur at about the same temperature in $Cs_2LiCo(CN)_6$. Thus, the structural change at approximately 183 K for $Cs_2LiCo(CN)_6$ involves both a discontinuous rotation of the $Co(CN)_6^{3-}$ octahedra and a continuous translation of the Cs^+ atoms.

The nature of the soft modes changes as the crystals are cooled well below T_c^2. The soft mode transforms as the totally symmetric representation in the lower symmetry phase.[27] However, in going to the low-temperature $P2_1/n$ cell, two other low-energy Cs^+ translations and three of the rotary modes also have A_g symmetry. As the energy of the soft mode approaches that of the other phonons of A_g symmetry, mode coupling is expected. It is likely, therefore, that the soft mode, which exclusively involves Cs^+ translation along the (110) cubic cell direction at T_c^2, will take on $M(CN)_6^{3-}$ rotational and other Cs^+ translational character at lower temperatures. The implication here is that the crystal can distort along any of the allowed A_g symmetry directions. This mode coupling in the "reaction path" is clearly illustrated in the room-temperature structures of $Cs_2NaFe(CN)_6$ and $Cs_2KFe(CN)_6$.[28] These materials crystallize in $P2_1/n$ at room temperature with significant distortions along all of the possible A_g symmetry coordinates (the critical temperatures for these materials are well above room temperature).

It has been suggested that the lattice instabilities in these materials is a result of the Cs^+ ion occupying too large a site.[5,7] In this regard, it is interesting to compare the critical temperatures for the $Cs_2LiM(CN)_6$ salts with the $Fm3m$ cell structural parameters (Table I). In going from Cr^{3+} through Co^{3+} the lattice size and Cs–N, Cs–C contact distances decrease monotonically.[23] As expected, the critical temperature decreases in the series $Cr^{3+} \rightarrow Co^{3+}$ indicating that the Cs^+ site size is the dominant factor in determining the structural instabilities. Raman studies of the isomorphous $Cs_2MFe(CN)_6$ ($M = Mg^{2+}$, Ca^{2+}, and Sr^{2+})[7] and $Cs_2NaLnCl_6$ (Ln = lanthanide)[29] support the suggestion that a smaller Cs^+ site size stabilizes the $Fm3m$ structure. Furthermore, replacement of Li^+ by Na^+ or K^+ in $Cs_2MFe(CN)_6$ gives stable crystals in $P2_1/n$ and raises the critical temperatures substantially.[30]

While the Cs^+ site size plays an important role in determining the critical temperature, it is clear from Table I that it is not the only factor. The Cs–N and Cs–C contact distances in $Cs_2LiIr(CN)_6$ are shorter than the corresponding distances in the Cr^{3+} salt, and yet the critical temperatures in $Cs_2LiIr(CN)_6$ are substantially higher than those in $Cs_2LiCr(CN)_6$. Interestingly, the Cs^+ thermal motion does correlate with the critical temperatures for all of the materials. Not surprisingly, the root-mean-square amplitudes of vibration appear to provide a better indication of the stability of the cubic phase.

It is not immediately clear why there is an inversion in the critical temperature for the Cr^{3+} and Ir^{3+} salts. The Li–N distances are the same for each material. Also, the difference in mass of the $M(CN)_6^{3-}$ ion cannot be important since the metal does not move during the course of the structural change and since the soft mode cannot involve $M(CN)_6^{3-}$ translation (above). The only real difference between these two salts is in the internal forces of the complex ion itself. With considerable temerity, we offer the following explanation.

Transition metal cyanide compounds are considered by many to be weak π-acceptor complexes.[31] There are clear indications that the degree of $d\pi$–$p\pi^*$ bonding in these materials increases in the series $Cr^{3+} \rightarrow Co^{3+}$ and also increases in going down the Co group.[23,32,33] Thus, we expect more electron density in the π^* CN^- orbitals in the Ir^{3+} salt than in the Cr^{3+} material. Additional electron density in the diffuse CN^- π^* orbitals could destabilize the Cs^+–CN^- interaction since the Cs^+ atom is nearly equidistant from the C and N atoms in the cubic cell. A structural distortion involving Cs^+ translation and $M(CN)_6^{3-}$ rotation could bring the Cs^+ atom into a more favorable position for σ-type Cs^+–CN^- interaction involving the π^* CN^- orbitals. In support of this explanation it is noted that the Cs–N and Cs–C contacts in the distorted $Cs_2NaFe(CN)_6$ and $Cs_2KFe(CN)_6$ structures are quite different. Irrespective of whether or not the difference in $d\pi$–$p\pi^*$ bonding results in the observed inversion of the Cr^{3+} and Ir^{3+} critical temperatures, the present results point to a fascinating cooperative interaction between external and internal forces.

In conclusion, there is increasing evidence that the structural instabilities first characterized in $Cs_2LiCr(CN)_6$ are a common feature of salts which possess the elpasoite structure. Quite simply, crystalline solids with similar structures share common lattice instabilities. It is also noted that the critical temperatures are determined largely by readily identified structural parameters—the relative tetrahedral ion/site sizes. This information could prove useful to those interested in studying O_h coordinated complex ions in the solid state where it is often necessary to control the symmetry of the ML_6^{n-} lattice site. These studies indicate that the ML_6^{n-} site symmetry is limited in elpasoite salts if the tetrahedral site is too large for the resident ion. The ML_6^{3-} site symmetries observed for the materials studied to date include O_h, C_{4h}, and C_{2h}.[5] Finally, it is noted that mechanistic information of lattice instabilities is of prime importance in the area of ionic conductivity. It would be extremely useful to be able to identify those structural features to build into a crystalline lattice to effect ion mobility—an important type of structural instability.

Acknowledgment. This work was supported by the Robert A. Welch Foundation (Grant No. 620).

Registry No. $Cs_2LiCo(CN)_6$, 23591-91-5; $Cs_2LiIr(CN)_6$, 42055-52-7.

References and Notes

(1) W. Cochran, *Phys. Rev. Lett.*, **3**, 521 (1959).
(2) W. Cochran, *Adv. Phys.*, **9**, 387 (1960); **10**, 401 (1961).
(3) J. F. Scott, *Rev. Mod. Phys.*, **46**, 83 (1974).
(4) R. L. Armstrong, *J. Magn. Reson.*, **20**, 214 (1975).
(5) R. R. Ryan and B. I. Swanson, *Phys. Rev. B*, **13** (12), 5320 (1976).
(6) B. I. Swanson, B. C. Lucas, and R. R. Ryan, *J. Chem. Phys.*, in press.
(7) J. J. Rafalko, B. I. Swanson, and G. W. Beall, *J. Solid State Chem.*, **21**, 195 (1977).
(8) B. I. Swanson, *Phys. Status Solidi A*, **47**, K95 (1978).
(9) R. L. Armstrong and H. M. vanDriel, *Can. J. Chem.*, **50**, 2048 (1972).
(10) G. P. O'Leary, *Phys. Rev. Lett.*, **23**, 782 (1969).
(11) R. L. Armstrong, G. L. Baker, and H. M. vanDriel, *Phys. Rev. B*, **3**, 3092 (1971).
(12) G. P. O'Leary, *Phys. Rev. B*, **3**, 3075 (1971).
(13) H. M. vanDriel, R. L. Armstrong, and M. M. McEnnan, *Phys. Rev. B*, **12**, 3072 (1975).
(14) R. H. Busey, H. H. Dearman, and R. B. Bevan, Jr., *J. Phys. Chem.*, **66**, 82 (1962).
(15) M. Wiszniewska and R. L. Armstrong, *Can. J. Phys.*, **51**, 781 (1973).
(16) H. M. vanDriel, M. Wiszniewska, B. M. Morres, and R. L. Armstrong, *Phys. Rev. B*, **6**, 1596 (1972).

(17) R. L. Armstrong and C. A. Martin, *Phys. Rev. Lett.*, **35**, 294 (1975).
(18) K. R. Jeffrey, *J. Magn. Reson.*, **7**, 184 (1972).
(19) A. Sasane, D. Nakamura, and M. Kubo, *J. Magn. Reson.*, **3**, 76 (1970); B. I. Swanson and B. C. Lucas, to be submitted for publication.
(20) B. I. Swanson and B. C. Lucas, to be submitted for publication.
(21) J. Rafalko, B. I. Swanson, and B. Schwartz, to be submitted for publication.
(22) J. F. Scott and J. P. Remeika, *Phys. Rev. B*, **1**, 4182 (1970).
(23) B. I. Swanson and R. R. Ryan, *Inorg. Chem.*, **12**, 285 (1973); R. R. Ryan and B. I. Swanson, *ibid.*, **13**, 1681 (1974).
(24) G. G. Schlessinger, *Chemist-Analyst*, **56**, 48 (1967).
(25) B. I. Swanson and L. H. Jones, *Inorg. Chem.*, **13**, 313 (1974).
(26) J. J. Rafalko, B. I. Swanson, and L. H. Jones, *J. Chem. Phys.*, **67**, 1 (1977).
(27) J. M. Worlock, Proceedings of NATO Advanced Study Institute, Structural Phase Transitions and Soft Modes, Geilo, Norway, April 1971, p 329.
(28) S. R. Fletcher and T. C. Gibb, *J. Chem. Soc., Dalton Trans.*, 309 (1977).
(29) R. W. Schwartz, S. F. Watkins, C. J. O'Connor, and R. L. Carlin, *J. Chem. Soc., Faraday Trans. 2*, **72**, 565 (1976).
(30) The critical temperature for the second phase change in $Cs_2NaFe(CN)_6$ was observed at 499 K via optical microscopy: B. Swanson unpublished results.
(31) L. H. Jones and B. I. Swanson, *Acc. Chem. Res.*, **9**, 128 (1976).
(32) B. I. Swanson, S. Hamburg, and R. R. Ryan, *Inorg. Chem.*, **13**, 1681 (1974).
(33) L. H. Jones, *Inorg. Chem.*, **2**, 777 (1963).

Contribution from Ames Laboratory, ERDA, Iowa State University, Ames, Iowa 50011, and the Department of Chemistry, Auburn University, Auburn, Alabama 36803

Polarized Single-Crystal Electronic Spectra for Tripotassium Tetrasulfatodimolybdate–3.5-Water

PHILLIP E. FANWICK,[1a] DON S. MARTIN, JR.,*[1a] THOMAS R. WEBB,[1b] GARY A. ROBBINS,[1a] and ROBERT A. NEWMAN[1a]

Received February 14, 1978

Low-temperature polarized spectra for the band of $K_3Mo_2(SO_4)_4 \cdot 3.5H_2O$ in the near-infrared region, between 5700 and 9000 cm^{-1}, are reported. This band has rather remarkable vibrational structure which provides an exceptional picture of vibrations in the excited state. The data are consistent with an assignment of the band as the $\delta^* \leftarrow \delta$, $^2B_{1u} \leftarrow {}^2B_{2g}$, dipole-allowed transition. The information, including hot bands developed in spectra above 80 K, indicate that the 0–0 lines of the two crystallographic sites are at 6311 and 6418 cm^{-1}. However, there is no observed splitting of symmetry-related crystal (Davydov) states. Extended Franck–Condon progressions for each site based on a metal–metal stretching vibration of 350 cm^{-1} are observed. In addition, Franck–Condon terms of three other vibrations are seen. There are also weak featureless bands in the visible region at 16 800 and 24 000 cm^{-1}.

Introduction

Single-crystal electronic absorption spectra have been reported by now for several compounds which contain dimeric complexes of transition elements with quadruple metal–metal bonds. Studies[2-4] of crystals with $Re_2Cl_8^{2-}$ together with results[5] for $Mo_2Cl_8^{4-}$ have confirmed that the lowest energy observed electronic absorption is polarized in the direction of the metal–metal bond. In the D_{4h} symmetry of the d^8 $M_2Cl_8^{n-}$ ion, the spin-allowed $\delta^* \leftarrow \delta$ transition involves the excitation $b_{1u}^* \leftarrow b_{2g}$, so the transition is $^1A_{2u} \leftarrow {}^1A_{1g}$ and should be dipole-allowed along the z axis which is coincident with the metal–metal bond. Therefore, this first transition can be reasonably assigned as $\delta^* \leftarrow \delta$. Such an assignment is predicted by $X\alpha$ scattered wave calculations,[3-6] although the calculated energies for the transition have rather generally been much lower than those observed.

Polarized crystal spectra[7] of $K_4Mo_2(SO_4)_4 \cdot 2H_2O$ have indicated a band with its maximum at 19 400 cm^{-1} and also a polarization consistent with a $\delta^* \leftarrow \delta$ assignment. On the other hand, the lowest energy electronic transitions in crystal spectra for the molybdenum alkylcarboxylate dimers[7-9] have exhibited much lower intensities. Vibrational structure for these absorption bands at liquid-helium temperature have indicated components in both the z and x,y polarizations which imply some excitation by vibronic (Herzberg–Teller) perturbations.

In the synthesis of the red $K_4Mo_2(SO_4)_4 \cdot 2H_2O$, blue crystals are frequently encountered,[10] especially if oxygen has not been rigorously excluded. In this compound, $K_3Mo_2(SO_4)_4 \cdot 3.5H_2O$, the $Mo_2(SO_4)_4^{4-}$ anion has been subjected to a one-electron oxidation to form the $Mo_2(SO_4)_4^{3-}$ anion. The crystal structure of both the red and blue compounds was reported by Cotton et al.,[11] and the present work was undertaken to obtain polarized crystal spectra for the oxidized dimeric anion. In the meantime, Gray and co-workers[12] have reported a richly structured absorption band for KBr pellets of $K_3Mo_2(SO_4)_4 \cdot 3.5H_2O$ in the near-infrared region between 1200 and 1600 nm which they tentatively assigned as the $\delta^* \leftarrow \delta$ transition.

Experimental Section

The preparation of $K_3Mo_2(SO_4)_4 \cdot 3.5H_2O$ has been described previously.[11] The compound crystallizes with a monoclinic lattice $C2/c$, $a:b:c = 30.654:9.528:12.727$, and $\beta = 97.43°$. A number of very thin crystals, suitable for spectroscopy, were found. Several crystals were mounted on the goniometer head of a computer controlled four-circle X-ray diffractometer. From preliminary oscillation photographs, the crystallographic axes were determined by standard programs to be in agreement with the reported values. From observations of the crystals as various reflections were called into the diffracting position, it was determined that the large faces of thin rectangular crystals were 100 with the c axis aligned in the direction of the long dimension. Other crystals in the form of prismatic needles had developed 100 and 010 faces. For the 100 face of monoclinic crystals, electric vectors of the two transmitted plane polarized light waves are exactly aligned with the b and c crystallographic axes so it has been possible to obtain absorption spectra for these b and c polarizations. The indices of refraction for the 100 face were determined for Na D to be $n_b = 1.581$ and $n_c = 1.552$ by the Becke line method with the use of calibrated immersion liquids purchased from the Cargille Co. The thickness for the crystals was determined from the interference colors between crossed polarizers and the indicated birefringence. The thickness of one crystal with optical faces could be confirmed as well by an interference method from the wavelengths of a series of absorbance maxima and minima in a region of low absorptions.[13] Uncertainty in the thickness was about 10%. For the near-infrared region, where detection is much less sensitive than in the visible and near-ultraviolet region, it was possible to find crystals with faces sufficiently large (0.5–1.0 mm) for the instrumental sensitivity and to mount these crystals over slits in metal plates so the long dimension could be aligned with the slit images in the sample compartment of the spectrophotometer.

The experimental procedures for measuring polarized spectra at liquid-helium temperatures have been described previously.[5,14] For the study of hot bands, the temperature of the sample holder was measured by means of a platinum resistance thermometer. The

0020-1669/78/1317-2723$01.00/0